The 2nd Int. Symp. on Turbulence and Shear Flow Phenomena, Vol 1, pp.359-364, Stockholm, 2001

A MODEL FOR ESTIMATING THREE-DIMENSIONAL BOUNDARY LAYERS IN ROTATING DUCT FLOW AT HIGH ROTATION RATES

J. Pallares, F. X. Grau
Department of Mechanical Engineering. University Rovira i Virgili
Ctra. Salou s/n 43006-Tarragona. Spain
pallares@etseq.urv.es, xgrau@etseq.urv.es

L. Davidson
Department of Thermo and Fluid Dynamics. Chalmers University of Technology
SE-412 96 Gothenburg. Sweden
lada@tfd.chalmers.se

ABSTRACT

Numerical simulations of flow in a rotating square duct at high rotation rates are presented. Computation and analysis of the different terms of the averaged momentum budget near the sidewalls have shown the dominant mechanisms of momentum transfer in these regions. A model for the velocities has been developed by analytically solving simplified versions of these budgets within the lateral three-dimensional boundary layers. The resulting predictions of the velocity profiles and the boundary layer quantities are in good agreement with present numerical results.

INTRODUCTION

Prediction and analysis of the effects of rotation on turbulent flows have been motivated mainly by their implications in engineering fields concerned with flow and/or heat transfer processes in rotating devices. Numerical and experimental studies dealing with rotating channel flows, subjected to rotation around an axis parallel to the spanwise direction, have shown that turbulent mixing of fluid particles is enhanced in the regions of the flow where the streamwise momentum is unstably stratified with respect to the Coriolis force (unstable side or pressure side) while a reduction of mixing is observed where the streamwise momentum is stably stratified (stable side or suction side) (Johnston et al., 1972; Kristoffersen and Andersson, 1993 and Alvelius, 1999). It should be noted that, here, the concept of stability is related to the augmentation (unstabilization) or reduction (stabilization) of the turbulence level of the flow caused by rotation. In finite aspect ratio ducts, Coriolis force generates persistent secondary flows, which contribute to the mixing processes between the stable and unstable side of the duct. Essentially, the time averaged secondary flows consist in two large counter-rotating cells that convect low momentum fluid from the stable side to the unstable side across the central region of the duct and from the unstable to the stable side along the sidewalls (Murata and Mochizuki, 1999 and Pallares and Davidson, 2000).

MODEL

The present study analyzes the flow in a rotating straight square duct at high rotation rates (Ω) using the large-eddy simulation (LES) technique. The smooth duct is rotating with respect to an axis parallel to the z direction, $\Omega = (0,0,\Omega)$, as indicated in figure 1. The flow, which is driven by an externally imposed pressure gradient, is assumed to be fully developed, incompressible and isothermal.

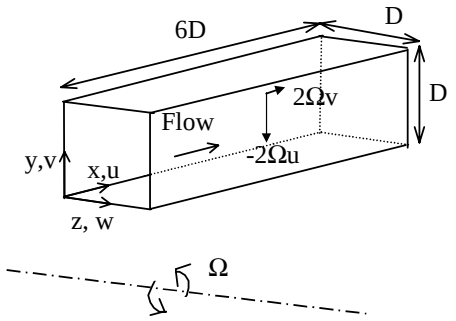

Figure 1: Physical model and coordinate system. The components of the Coriolis acceleration are also indicated.

The large-eddy simulation (LES) technique has been chosen to keep the computational requirements at a moderate level. LES is based on decomposition of the flow variables into a large-scale (or resolved) component and a subgrid scale component. The resolved scales and the corresponding governing transport equations are defined by the filtering operation. The non-dimensional filtered continuity and Navier-Stokes equations are

$$\frac{\partial u_i}{\partial x_i} = 0 \qquad (1)$$

and

$$\frac{\partial u_i}{\partial t}+\frac{\partial u_j u_i}{\partial x_j}=4\delta_{1j}-\frac{\partial p}{\partial x_i}-\frac{\partial \tau_{ij}}{\partial x_j}+ \\ +\frac{1}{Re_\tau}\frac{\partial^2 u_i}{\partial x_j \partial x_j}+\in_{ij3} Ro_\tau u_j \qquad (2)$$

respectively.

The scales used to obtain the non-dimensional variables are the hydraulic diameter (D) and the average friction velocity (u_τ). Pressure is scaled with the average wall shear stress, ρu_τ^2. The different terms on the right hand side of equation (2) are, from left to right, the imposed non-dimensional pressure gradient along the streamwise direction, the gradient of the fluctuating pressure, the subgrid scale contribution, the viscous diffusion term and the Coriolis term. Figure 1 shows the direction of the components of the Coriolis force according to the system of coordinates adopted. The centrifugal acceleration, which is considered constant, is included in the non-dimensional mean pressure gradient. In equation (2), $\in$ is the Levi-Civita´s alternating tensor, $Re_\tau = u_\tau D/\nu$ and $Ro_\tau = 2\Omega D/u_\tau$, are the Reynolds and the rotational numbers, respectively.

The Reynolds number based on the hydraulic diameter of the duct and the averaged friction velocity has been kept constant, Re_τ=300, (i.e. constant imposed pressure gradient) in the range of rotation numbers studied ($3 \le Ro_\tau \le 40$). The numerical simulations were carried out with the CALC-LES code, a finite volume second order accuracy code, using the localized one-equation dynamic subgrid-scale (SGS) model proposed by Kim and Menon (1997). The details about the code can be found in Sohankar et al. (2000). The computation of the SGS stresses using a localized dynamic procedure is an important feature when simulating rotating turbulent flows because of the stabilizing/destabilizing effects of rotation on turbulence. In the present simulations, the localized dynamic SGS model predicts a negligibly small SGS viscosity, in comparison with the molecular viscosity, in the regions where the flow has been relaminarized by the effect of rotation. LES of stationary duct flow and rotating channel flow were initially carried out and results were in good agreement with existing experimental and direct numerical simulation data (Pallares and Davidson, 2000)

The non-slip boundary condition was applied at the four walls and periodic boundary conditions were used at the inlet and outlet of the duct. The computational domain (L_x=6D, L_y=L_z=D) was divided into 66x66x66 grid nodes. The grid nodes were stretched near the wall using a tanh function and uniformly distributed along the homogeneous streamwise direction (Δx^+=29). For the Reynolds number considered, Re_τ=300, the minimum and maximum grid spacing in the directions perpendicular to the walls are $(\Delta y+)_{min}$= $(\Delta z^+)_{min} \approx 0.4$ and $(\Delta y^+)_{max}$= $(\Delta z^+)_{max} \approx 9$.

RESULTS AND DISCUSSION

Mean flow fields

In the simulations, the averaging procedure was started when the flow was statistically fully developed. Flow quantities were averaged along the homogeneous x-direction as well as in time, typically during 50-70 non-dimensional time units. Time and x-direction averaged flow fields progressively tended to be symmetric with respect to z=0.5 as the sampling size was increased. Consequently, symmetry of the mean flow field with respect to z=0.5 was enforced in order to increase the sampling size.

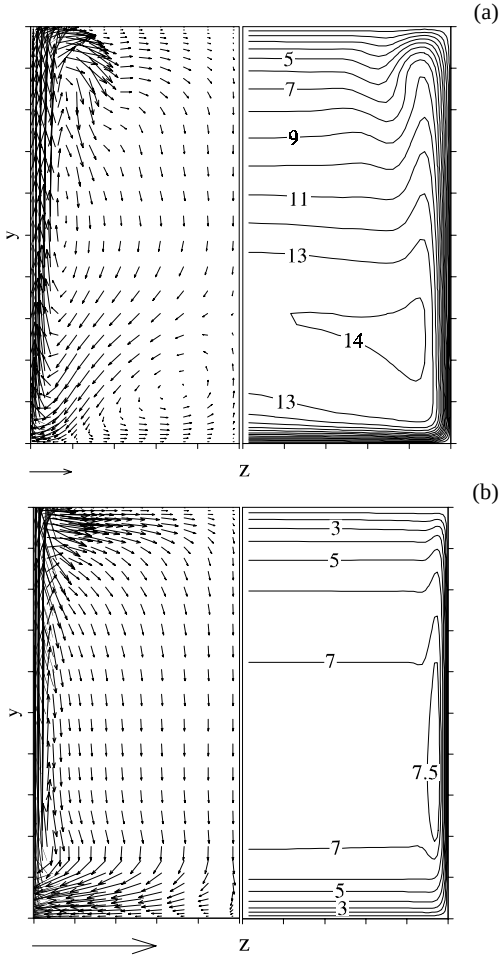

Figure 2 : Averaged cross-stream vector fields and streamwise velocity component contours at Re_τ=300 and (a) Ro_τ=3 and (b) Ro_τ=40. The vectors near the bottom left corners have length 1.

Figures 2.a and 2.b show the average flow fields at Ro_τ=3 and Ro_τ=40, respectively. In these figures, the cross-stream vector fields are represented on the left

while the streamwise velocity contours are depicted on the right. On the left part of Figures 2.a and 2.b only every second vector is shown.

The effects of low rotation rates ($0 \le Ro_\tau \le 1.5$) in turbulent duct flow at $Re_\tau=300$ were investigated by Pallares and Davidson (2000). These authors found that at $Ro_\tau=1.5$, the turbulence intensities of the flow are concentrated near the unstable wall (y=0) and near the sidewalls (z=0 and z=1). The flow can be considered laminar in the central part of the duct where cross-stream convection of x-momentum from the stable side to the unstable side produce the stabilization of the flow to a Taylor-Proudman regime (i.e., the streamwise velocity component does not vary along the direction of the axis of rotation). Figure 3 shows the evolution of the non-dimensional volume averaged turbulent kinetic energy, $\langle K \rangle_V$, scaled with the bulk velocity (U_b) as a function of the rotational number. The important reduction of $\langle K \rangle_V$ in the range $1.2 < Ro_\tau \le 3$ corresponds to the decrease of the streamwise Reynolds stress component which receives energy from the main shear stresses ($\partial u/\partial y$ and $\partial u/\partial z$). For example, the reduction of $\langle K \rangle_V$ at $Ro_\tau=1.5$ (Re=3900) is 48% and at $Ro_\tau=3$ (Re=3420) is 73%, with respect to the volume averaged turbulent kinetic energy of the non-rotating case (Re=4500). Note that the increase of the rotational number produces a reduction of the Reynolds number ($Re=Re_\tau\ U_b$) based on the bulk velocity, if, as in the present simulations, Re_τ is kept constant (i.e., constant imposed pressure gradient along the x-direction).

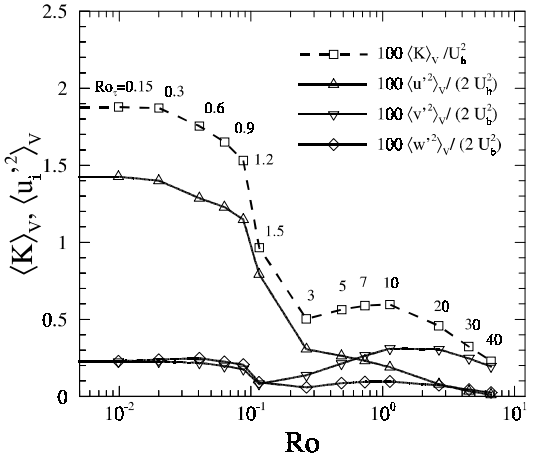

Figure 3 : Volume averaged turbulent kinetic energy as a function of the rotational number $Ro=Ro_\tau/U_b$. The values of Ro_τ are indicated near the corresponding symbols. Data from Pallares and Davidson (2000) in the range $0 < Ro_\tau \le 1.5$ is also included in this figure.

The topology of the average flow field at $Ro_\tau=3$, shown in Fig 2.a, is similar to that reported in Pallares and Davidson (2000) at $Ro_\tau=1.5$. The averaged cross-stream vector field consists in two large stretched secondary flows near the sidewalls (z=0 and z=1) and two small secondary cells near the unstable wall (y=0). The increase of the rotation number from $Ro_\tau=1.5$ (Re=3900) to $Ro_\tau=3$ (Re=3420) produces the enlargement of the small secondary cells and a displacement of maxima of the axial velocity component towards the sidewalls (see figure 2.a). These changes in the mean flow field near the unstable wall can be attributed to the reduction of the Reynolds number, which produces transition of the boundary layer near the unstable wall.

Figure 3 shows that, in the range $7 \le Ro_\tau \le 40$, the vertical component of the Reynolds stress tensor, $\langle v'^2 \rangle$, is the main contributor to the unsteadiness of the flow. As shown in figure 2.b, at the highest rotation rate ($Ro_\tau=40$) the secondary flow which consists in two large stretched cells generates thin three-dimensional boundary layers near the sidewalls. These boundary layers are the major contributors to the overall head loss of the flow as can be inferred from the concentration of the contour levels near the sidewalls in figure 2.b.

Averaged momentum budgets

In this section a model to predict the velocities and the head loss produced by the three-dimensional boundary layers developed at the sidewalls is presented. This model is based on the analytical solution of the simplified averaged momentum budgets. The non-dimensional averaged x- and y-momentum budgets can be written as,

$$-\left(V\frac{\partial U}{\partial y}+W\frac{\partial U}{\partial z}\right)+\frac{1}{Re_\tau}\left(\frac{\partial^2 U}{\partial y^2}+\frac{\partial^2 U}{\partial z^2}\right)-\left(\frac{\partial\langle u'v'\rangle}{\partial y}+\frac{\partial\langle u'w'\rangle}{\partial z}\right)+Ro_\tau V+SGS_U=-4 \quad (3)$$

$$-\left(V\frac{\partial V}{\partial y}+W\frac{\partial V}{\partial z}\right)+\frac{1}{Re_\tau}\left(\frac{\partial^2 V}{\partial y^2}+\frac{\partial^2 V}{\partial z^2}\right)-\left(\frac{\partial\langle v'^2\rangle}{\partial y}+\frac{\partial\langle v'w'\rangle}{\partial z}\right)-Ro_\tau U+SGS_V=\frac{\partial P}{\partial y} \quad (4)$$

The different terms in equations (3) and (4) are responsible, from left to right, for the convective, viscous and turbulent momentum transport. The fourth and the fifth terms are the Coriolis force and the SGS transport. The terms on the right side of equations (3) and (4) represent the average pressure gradient along the x- and y-directions, respectively.

Figures 4.a and 4.b shows the terms of the momentum budgets, as they appear in equations (3) and (4), along the line y=0.5 at the highest rotation rate analyzed in this study ($Ro_\tau=40$). The SGS terms make no significant contribution to the momentum budgets shown in Figure 4 and have been omitted. It

can be seen in Figure 4.a that the imposed pressure gradient along the x-direction is balanced by the viscous diffusion along the z direction and the Coriolis term. Figure 4.a allows to rewrite equation (3) near the sidewalls as

$$\frac{1}{Re_\tau}\left(\frac{\partial^2 U}{\partial z^2}\right)+Ro_\tau V \approx -4 \qquad (5)$$

and in the central part of the duct as

$$Ro_\tau V_c \approx -4\,. \qquad (6)$$

Note that the vertical velocity component is approximately constant in the central part of the duct (see Fig. 4) and is denoted in equation (6) as V_c, $V_c \approx -4/Ro_\tau$.

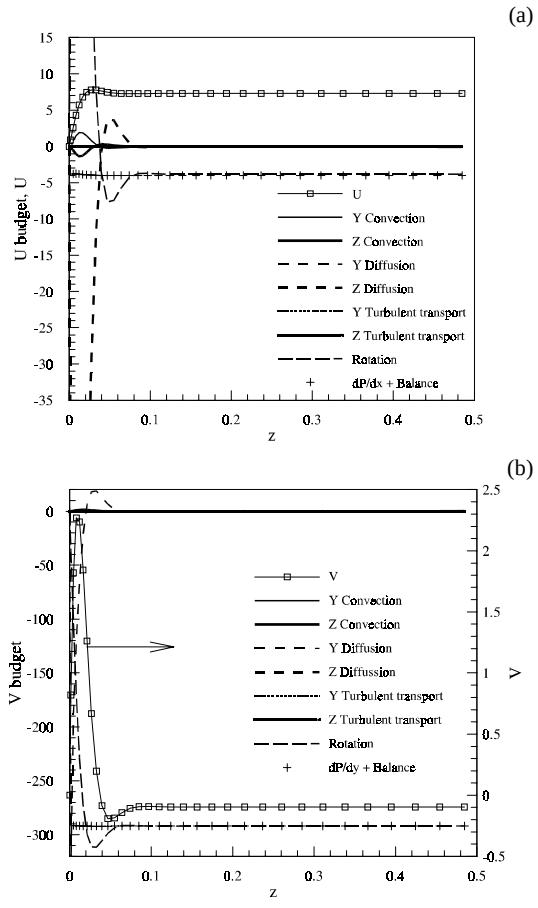

Figure 4 : Averaged x- (a) and y-momentum (b) budgets along the line y=0.5 at Re_τ=300 and Ro_τ=40. The corresponding velocity profiles are also included in this figure. In figure 4.b the vertical axis for V is on the right.

Similarly, the simplified y-momentum budgets near the sidewalls and in the central part of the duct are

$$\frac{1}{Re_\tau}\left(\frac{\partial^2 V}{\partial z^2}\right)-Ro_\tau U \approx \frac{\partial P}{\partial y} \qquad (7)$$

and

$$-Ro_\tau U_c \approx \frac{\partial P}{\partial y} \qquad (8)$$

respectively. Figure 4.b shows that pressure does not depend on z indicating that the W velocity component is negligibly small compared with V. Inspection of the momentum budgets at high rotation rates and at different y positions shows that equations (5) to (8) are valid approximations of the complete momentum budgets in most of the cross section of the duct, as can be inferred from the flow topology in figure 2.b.

Rearranging equations (7) and (8), the simplified y-momentum budget can be written as

$$\frac{1}{Re_\tau}\left(\frac{\partial^2 V}{\partial z^2}\right)-Ro_\tau(U-U_c)\approx 0 \qquad (9)$$

The boundary conditions for equations (5) and (9) are z=0, U=0, V=0 and z=0.5, $\partial U/\partial z=0$, $\partial V/\partial z=0$. The solutions to equations (5) and (9) and the corresponding boundary conditions can be expressed as,

$$U = U_c\left(1-\cos(a\,z)e^{-a\,z}\right)-V_c\left(\sin(a\,z)e^{-a\,z}\right) \quad (10)$$

$$V = V_c\left(1-\cos(a\,z)e^{-a\,z}\right)+U_c\left(\sin(a\,z)e^{-a\,z}\right) \quad (11)$$

where a is a constant related with the Ekman number ($Ek=\nu/\Omega D^2$), $a=\sqrt{Ro\,Re/2}=1/\sqrt{Ek}$. Note that the only unknown parameter in equations (10) and (11) is the streamwise velocity component in the center of the duct, U_c, since $V_c=-4/Ro_\tau$. It can be seen in figure 5 that the numerically predicted velocity profiles at Ro_τ=40 along the line y=0.5 agree with the analytical solutions using the value of U_c obtained in the simulations. A similar agreement between the analytical solutions and the numerical results is found in the range 0.15<y<0.85.

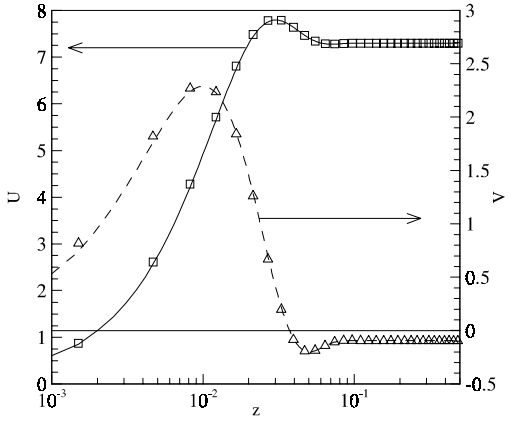

Figure 5 : Velocity profiles along the line y=0.5 at Ro_τ=40. Symbols: Numerically predicted profiles. Lines: Analytical solutions

The use of equations (10) and (11) to predict the velocity profiles is subjected to the validity of the simplified momentum budgets in equations (5), (6) and (9). These equations express the balance between the pressure gradient terms and the Coriolis force in the central part of the duct where the flow has been relaminarized by the effect of rotation. At moderate rotation rates ($1.5 \le Ro_\tau \le 10$) the vertical convection of x-momentum ($-V\partial U/\partial y$) contributes, in the central part of the duct, together with the Coriolis term (Ro_τ V) to balance the imposed pressure gradient along the x-direction. For example the ratio $(-V\partial U/\partial y)/(Ro_\tau V)$ is about 12 at $Ro_\tau=1.5$, 0.9 at $Ro_\tau=10$, 0.2 at $Ro_\tau=20$ and 0.03 at $Ro_\tau=40$.

Consequently, equations (10) and (11) can be used to estimate boundary layer quantities for $Ro_\tau \ge 20$. For example, the boundary layer thicknesses defined as the distance from the wall to the position of the maximum velocity are for U, $\delta_U \approx 3\pi Ek^{1/2}/4$ and for V, $\delta_V \approx \pi Ek^{1/2}/4$. The ratio between the non-dimensional secondary flow rate per unit length (Q_V) pumped by the Coriolis force and the bulk velocity is,

$$\frac{Q_V}{U_b} = \frac{2}{U_b} \int_{z=0}^{\delta_{V=0}} V \, dz \approx \frac{\sqrt{Ek}}{1-\sqrt{Ek}} \qquad (12)$$

where $\delta_{V=0} \approx \pi\, Ek^{1/2}$ is the non-dimensional distance from the sidewall to the position where V=0 (see figure 5). In equation (12) U_b is the non-dimensional bulk velocity ($U_b = \overline{U}_b / u_\tau$) and can be expressed as,

$$U_b \approx 2 \int_0^{0.5} U \, dz \approx U_c \left(1-\sqrt{Ek}\right). \qquad (13)$$

Equation (13) assumes that the velocity profiles, along the z direction, given in equations (10) and (11) are valid for most of the cross section of the duct.

Figure 6 shows the overall friction factor ($Cf = 2\tau_w / \rho \overline{U}_b^2$) and the local friction factors at the unstable (y=0, Cf_u), stable (y=1, Cf_s) and lateral walls (z=0 and z=1, Cf_l) as a function of $Ek^{1/2}$. Local friction factors are based on the main shear stress averaged along the wall. Note that by definition, $Cf = Cf_u + Cf_s + Cf_l$. It can be seen that the local friction factor corresponding to the sidewalls is the main contributor to the total head loss at high rotation rates. At $Ro_\tau=40$, the average wall shear stress associated with the boundary layers near the two lateral walls is responsible for the 80% of the total head loss.

The definition of Cf_l, i.e. the sum of the friction coefficients of both sidewalls, can be rewritten in terms of the velocity gradient at the wall, which can be calculated using the velocity profile given in equation (10).

$$Cf_l = \frac{(\tau_w)_l}{\rho \overline{U}_b^2} = \frac{1}{Re\, U_b} \left.\frac{dU}{dz}\right|_{z=0} \approx \frac{1}{Re\sqrt{Ek}} \qquad (14)$$

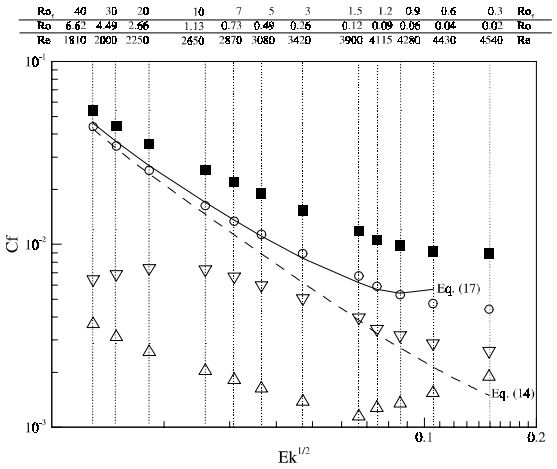

Figure 6 : Overall and local friction factors in a rotating square duct. Filled symbols: Overall friction factor. Open symbols: Average local friction factors at the sidewalls z=0 and z=1 (o), at the unstable wall y=0 (∇) and at the stable wall y=1 (Δ). The lines show the predictions of the friction factors of equations (14) and (17). The values of Ro_τ, $Ro=Ro_\tau/U_b$ and $Re=Re_\tau\, U_b$ are also included at the top of the figure.

Figure 6 shows that equation (14) provides a good estimation of Cf_l in the range $Ro_\tau \ge 20$ according to the fact that in this range a balance between the Coriolis force and the imposed pressure gradient is established in most of the area of the cross section of the duct.

An estimation of the overall friction factor at the sidewalls can be obtained rewriting equation (6) as,

$$Cf = -\frac{1}{2} Ro \frac{Vc}{U_b}. \qquad (15)$$

The ratio Vc/Ub in equation (15) can be obtained from global continuity of the secondary flow.

$$\frac{Vc}{U_b} = \frac{Q_V / U_b}{1 - 2\,\delta_{V=0}} \qquad (16)$$

Substituting equation (16) in (15) and using the approximate expression for Qv given in equation (12), Cf can be written as,

$$Cf \approx \frac{1}{Re\sqrt{Ek}} \frac{1}{\left(1-2\pi\sqrt{Ek}\right)\left(1-\sqrt{Ek}\right)} \qquad (17)$$

As shown in figure 6, equation (17) underpredicts the overall friction factor (Cf) by about a 15% in the range $Ro_\tau \ge 20$. It should be noted that the apparent agreement found in figure 6 between the numerically predicted local friction factor at the sidewalls and the

overall friction factor given in equation (17) has no theoretical basis, following the assumptions and procedures described above.

The final conclusions are that, at high rotation rates, equation (14) constitutes a good approximation to compute the friction factor at the lateral walls and that equation (17) gives a reasonable prediction of the overall friction factor for rotation dominated duct flows.

ACKNOWLEDGMENTS

Part of this work was carried out during the first author's visit at Chalmers in summer 2000. This work was financially supported by the Department of Thermo and Fluid Dynamics (Chalmers University of Technology) and by the Spanish Ministry of Science of Technology under project DPI2000-1578-C02-01.

REFERENCES

Alvelius, K., 1999 "Studies of turbulence and its modelling through large eddy- and direct numerical simulation", Ph.D. thesis, Department of Mechanics, Royal Institute of Technology, Stockolm.

Johnston, J. P., Hallen, R. M. and Lezius, D. K., 1972, "Effects of spanwise rotation on the structure of two-dimensional fully developed turbulent channel flow", J. Fluid Mech. vol. 56, p. 533

Kim, W. and Menon, S., 1997, "Application of the localized dynamic subgrid-scale model to turbulent wall-bounded flows" AIAA Paper 97-0210. 35th Aerospace Sciences Meeting & Exhibit, Reno, NV

Kristoffersen, R. and Andersson, H., 1993, "Direct simulations of low-Reynolds-number turbulent flow in a rotating channel", J. Fluid Mech. vol. 256, p. 163

Murata, A. and Mochizuki S., 1999, "Effect of cross-sectional aspect ratio on turbulent heat transfer in an orthogonally rotating rectangular smooth duct" Int. J. Heat Mass Transf. vol 42 p. 3803

Pallares J. and Davidson L., 2000, "Large-eddy simulations of turbulent flow in a rotating square duct", Phys. Fluids A vol. 12 (11) p. 2878

Sohankar, A., Davidson, L. and Norberg, C., 2000, "Large eddy simulation of flow past a square cylinder: Comparison of different subgrid scale models", J. Fluids Eng. vol. 122 p. 39. See also Erratum J. Fluids Eng. vol. 122 p. 643